Anatomic Considerations, Nomenclature, and Advanced Cross-sectional Imaging Techniques for Visualization of the Cranial Nerve Segments by MR Imaging

Ari M. Blitz, MD[a,*], Asim F. Choudhri, MD[b], Zachary D. Chonka, MD[a], Ahmet T. Ilica, MD[a], Leonardo L. Macedo, MD[c], Avneesh Chhabra, MD[d], Gary L. Gallia, MD, PhD[e], Nafi Aygun, MD[a]

KEYWORDS

• Cranial nerve segments • Cross-sectional imaging • MR imaging

KEY POINTS

- The cranial nerves (CNs) pursue a complex course through tissues with widely varying MR imaging signal characteristics as they extend from brainstem nuclei into the fluid-filled subarachnoid spaces and ultimately pass through the skull base to exit the cranium.
- In turn, the reported success of the variety of available MR imaging sequences for visualization of the CNs depends largely on their anatomic context at the point of evaluation.
- Consideration of the general segmental architecture of the CNs aids in evaluation of patients with pathologic conditions affecting or adjoining their course.

INTRODUCTION

The 12 pairs of cranial nerves (CNs) arise directly from the brain within the cranial vault (with the exception of spinal rootlets of CN XI, which arises from the rostral cervical spine). The CNs serve a variety of highly specialized functions, including those necessary for vision, movement of the eyes and face, and identification and consumption of food. The branching patterns and/or proximity of CNs to each other at points along their course may allow localization of pathology on clinical grounds.[1] MR imaging plays an important role in the localization and identification of pathology as well as presurgical planning. A variety of modalities have been used in the imaging evaluation of CNs. Clinically, the first cross-sectional imaging study to directly demonstrate the CNs was pneumoencephalography. During pneumoencephalography, the introduction of subarachnoid air surrounding the CNs allowed for visualization of the optic, oculomotor, trigeminal, and hypoglossal nerves within the basal cisterns.[2] The

[a] Division of Neuroradiology, The Russell H. Morgan Department of Radiology and Radiologic Science, The Johns Hopkins Hospital, Phipps B-100, 600 North Wolfe Street, Baltimore, MD 21287, USA; [b] Department of Radiology, University of Tennessee Health Science Center, Le Bonheur Neuroscience Institute, Le Bonheur Children's Hospital, 848 Adams Avenue-G216, Memphis, TN 38103, USA; [c] Cedimagem/Alliar, Diagnostic Center, 150 Centro, Juiz de Fora, Minas Gerais 36010-600, Brazil; [d] The University of Texas Southwestern, 5323 Harry Hines Blvd, Dallas, TX 75390-9178, USA; [e] Department of Neurosurgery, Neurosurgery Skull Base Surgery Center, The Johns Hopkins Hospital, Phipps 101, 600 North Wolfe Street, Baltimore, MD 21287, USA
* Corresponding author.
E-mail address: Ablitz1@jhmi.edu

Neuroimag Clin N Am 24 (2014) 1–15
http://dx.doi.org/10.1016/j.nic.2013.03.020
1052-5149/14/$ – see front matter

advent of CT enabled visualization of the region of the CNs with a greater degree of detail and with injection of intrathecal contrast; the CNs were visualized as linear filling defects within the subarachnoid space.[3] In both pneumoencephalography and CT cisternography, visualization was principally limited to the cisternal/subarachnoid course of the CNs and pathology was implied by alterations in the adjacent osseous structures. With the advent of MR imaging, cross-sectional examination of the structures of the head and neck without ionizing radiation became possible, with the ability to acquire images in any arbitrary plane allowing for the examination to be tailored to the CN in question. MR imaging is now the standard mode of imaging of the CNs and is the focus of this article.

TECHNICAL CONSIDERATIONS FOR MR IMAGING ACQUISITION FIELD STRENGTH

Fischbach and colleagues[4] studied T2-weighted spin-echo imaging of the CNs at 1.5T and 3T, the two most commonly available field strengths of clinical MR imaging units, and found that images acquired at higher spatial resolution on the 3T scanner nonetheless also had higher clarity and signal-to-noise ratio. The detection of perineural spread of neoplastic disease in the face initially not detected on 1.5T evaluation was possible on repeat examination at 3T.[5] Such results are not generally surprising because the tissue discrimination generally improved with higher field strengths.[6] Although 3T evaluation is generally preferred over 1.5T evaluation, diagnostic images may be obtained at either field strength, in particular when 3T MR imaging is not available, of questionable safety, or otherwise deemed inappropriate.

COIL CHOICE

Various approaches to coil choice and combination have been advocated[7] although phased-array head coils are typically used in the clinical setting and are adequate for most applications.

VOXEL SIZE AND COVERAGE

Thin-section imaging significantly improves detection of the CNs[8] although visualization of the cisternal trochlear (CN IV), abducens (CN VI), and accessory (CN XI) nerves may remain challenging. Due to its small caliber and proximity to multiple vascular structures, visualization of CN IV is particularly dependent on the spatial resolution of the sequences acquired. Choi and colleagues[9] compared conventional resolution (0.67 mm × 0.45 mm × 1.4 mm) to high-resolution (0.3 mm × 0.3 mm × 0.25 mm) imaging for detection of the cisternal trochlear nerve and found that the rate at which the nerve could probably or definitely be identified rose significantly from approximately 23% to 100%. **Fig. 1** demonstrates visualization of the trochlear nerve on 0.4-mm, 0.5-mm, and 0.6-mm isotropic constructive interference in the steady-state (CISS) images. Although increasing spatial resolution may improve visualization of small structures, the trade-off with respect to length of acquisition, reduced coverage, and/or decreased signal-to-noise ratio renders optimal coverage in all cases difficult. In the authors' practice, multiple 3-D sequences are typically used and include CISS imaging for the highest spatial resolution acquisition. The typical CISS acquisition includes 0.6-mm isotropic voxels with coverage of the entirety of the posterior fossa, skull base, and upper face. In select cases where CN IV palsy has been clinically diagnosed, a higher spatial resolution is often used.

2-D VERSUS 3-D IMAGING

Initially, MR imaging tailored to the CNs required careful attention to 2-D slice angulation to best demonstrate the CN in question.[10] Modern MR imaging equipment allows 3-D acquisition from

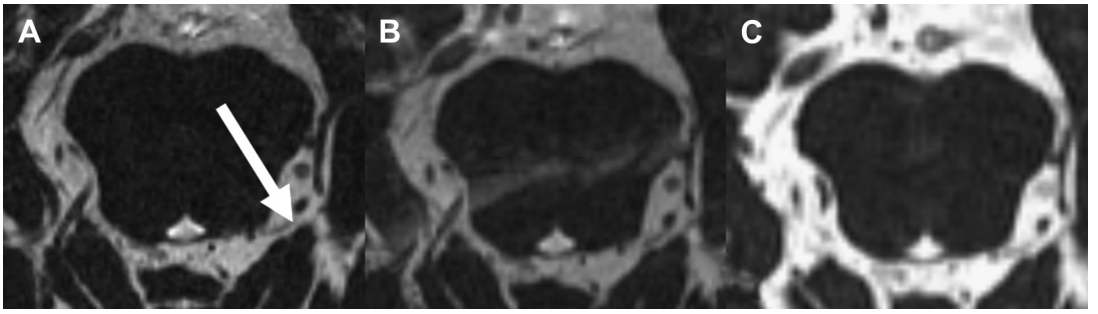

Fig. 1. Axial CISS images through the lower midbrain acquired at (*A*) 0.4-mm, (*B*) 0.5-mm, and (*C*) 0.6-mm isotropic resolution. The proximal cisternal CN IV, the obliquely oriented structure marked with an arrow (*A*), is progressively less well visualized as voxel size increases.

which post hoc reconstruction in multiple planes can be created, often better demonstrating the CNs.[8,11,12] One study of the cisternal components of the CNs in the cerebellopontine angle cistern with fast spin-echo technique found that 3-D imaging was superior to 2-D imaging due to suppression of flow artifacts and thinner sections and suggested that MR imaging evaluation of the cisterns be performed with 3-D technique.[13] When isotropic 3-D images are acquired, post hoc reconstructions can be made in any arbitrary plane, which is often useful in evaluating the complex anatomy of the CNs and surrounding structures.

INJECTION OF INTRAVENOUS CONTRAST AGENTS

The central nervous system (CNS) components of the CNs (including the entirety of the ophthalmic (CN I) and optic (CN II) nerves, which are properly tracts of the CNS rather than nerves per se) are at least partly isolated from the contents of the bloodstream by the blood-brain barrier and do not normally demonstrate visible contrast enhancement. The components of the CNs in the peripheral nervous system (PNS) are likewise separated by the blood-nerve barrier. When there is disruption of the blood-nerve barrier or blood-brain barrier, it is detected by the presence of an increase in intensity on postcontrast MR images with T1 weighting. Perhaps owing to lack of a similar barrier mechanism or increased blood flow, enhancement of the ganglia of the CNs may be detected as a physiologic finding.[14] Additionally, a circumneural arteriovenous plexus surrounds portions of the CNs in the interdural and foraminal regions of the skull base. Enhancement of the arteriovenous plexus may be seen, for instance, in the region of the tympanic and mastoid segments of the facial nerve (CN VII) in addition to the region of the geniculate ganglion.[15] Enhancement in the other CN components is pathologic. When present pathologic enhancement aids in the detection/localization of pathologic conditions of the CNs such as neoplastic, infectious, or inflammatory diseases.[16]

NOMENCLATURE

International consensus on anatomic nomenclature has been established in the *Terminologia Anatomica*.[17] The accepted terms for the CNs are olfactory nerve (CN I), optic nerve (CN II), oculomotor nerve (CN III), trochlear nerve (CN IV), trigeminal nerve (CN V), abducens or abducent nerve (CN VI), facial nerve (CN VII), vestibulocochlear nerve (CN VIII), glossopharyngeal nerve (CN IX), vagus nerve (CN X), accessory nerve (CN XI), and hypoglossal nerve (CN XII). The system defines multiple named subcomponents of the CNs by function. Structures with a single function and without branches, such as CN VI, receive no further subclassification. The international nomenclature incompletely serves the needs of a radiologist or clinician. For instance, lesions in various locations along the course of CN VI, although presenting with a similar clinical deficit of abduction of the globe, may have vastly differing differential diagnostic and clinical implications. Therefore, the authors propose a systematic method of segmental imaging evaluation of the CNs.

ANATOMIC SEGMENTS

After emerging from the brain, each of the CNs courses through the cerebral spinal fluid (CSF) before it traverses the meninges, extending through an associated skull base foramen to emerge into the head and neck. Along this path, the nerves are surrounded by CSF in the subarachnoid space, venous blood in the interdural compartment, bone within the skull base foramina, and various soft tissues after exiting from the skull. Although the anatomic course of each of the CNs is different, some fundamental anatomic considerations are sufficiently similar to allow a systematic classification of different segments, which share similar imaging properties (**Fig. 2**). General anatomic and imaging considerations for each segment follow. Selected information on pathology is included for illustrative purposes, although a comprehensive description of pathology affecting each segment is beyond the scope of this article.

a. Nuclear Segment

Anatomic considerations

The CN nuclei contain the cell bodies of neurons that either give rise to the efferent fibers, which

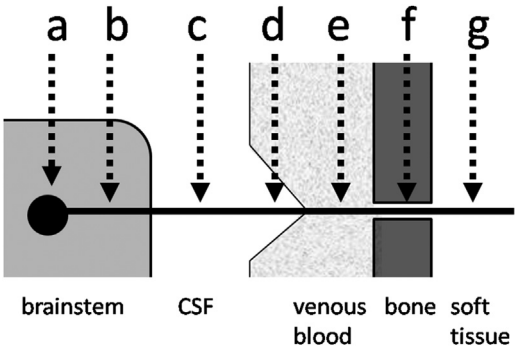

Fig. 2. Anatomic segments of the CNs with surrounding tissue (a, nuclear; b, parenchymal fascicular; c, cisternal; d, dural cave; e, interdural; f, foraminal; and g, extraforaminal).

exit the brainstem or receive afferent input. The CN nuclei extend from the midbrain (CN III) cranially into the rostral cervical spine caudally (CN XI).[18,19] The afferent nuclei generally rest lateral and dorsal to their efferent counterparts. Nuclei are further separated by their functional and evolutionary relationships from the somatic, branchial, and visceral (autonomic) motor nuclei. The visceral, somatic, and special sensory nuclei are arranged in columns approximately medial to lateral.[20]

Imaging approaches

In the fetal and neonatal brain, MR imaging allows direct identification of several CN nuclei, because the nucleus and proximal fibers myelinate earlier than the surrounding mesencephalic and rhombencephalic white matter tracts, best seen on T2-weighted imaging (**Fig. 3**).[21] Direct visualization of CN nuclei in the mature brain is difficult, and identification of pathology that has an impact on the nuclei requires knowledge of the location and function of the nuclei. The location of CN II.a, the lateral geniculate nuclei, can be directly seen as a focal protrusion on the posterolateral thalamus. The location of CN VI.a within the dorsal pons can be deduced when the facial colliculus is visualized (a name earned due to the traversing motor fibers of CN VII.b). The locations of components of CN V.a are reported as visible using diffusion tensor imaging (DTI) in the research setting.[22]

Selected pathologic entities

Most acquired pathologic conditions that have an impact on CN nuclei are related to regional abnormalities as opposed to abnormalities specific to the nucleus itself; thus, any process that has an impact on the adjacent brain parenchyma can have an impact on the nucleus of the CNs. Stroke, inflammatory processes, infection, tumor, and metabolic disorders, for instance, can result in nuclear-based cranial neuropathies.

b. Parenchymal Fascicular Segment

Anatomic considerations

The parenchymal fascicular segment runs from the point fibers exit the nuclei through the parenchyma to the point of separation from the brainstem at the apparent origin (AO). With the exception of CN IV.b, which alone exits the brainstem along the dorsal surface (see **Fig. 1**), the parenchymal fascicles of the CNs (also known as the CN tracts) pursue an anterior and lateral course through the brainstem to exit its ventral surface. Before separating from the brainstem to enter the cisternal segment, the CN fascicles may course along the surface of the brainstem. The point at which a discrete fascicle emerges from the parenchyma is known as the root exit point and the fascicular component, which may then course on the surface of the brainstem, is known anatomically as the attached segment (AS).[23,24] Studies in mammals demonstrate that these emergent fibers largely retain central myelination by oligodendrocytes before separating from the brainstem within the cisternal segment[25]; there are similar findings in humans.[23]

Imaging approaches

T2-weighted imaging The normal course of the fascicles of CN fibers extending from the nuclei toward the surface of the brainstem can sometimes be seen (see **Fig. 3**B) during the process of myelination in fetal or neonatal life using T2-weighted

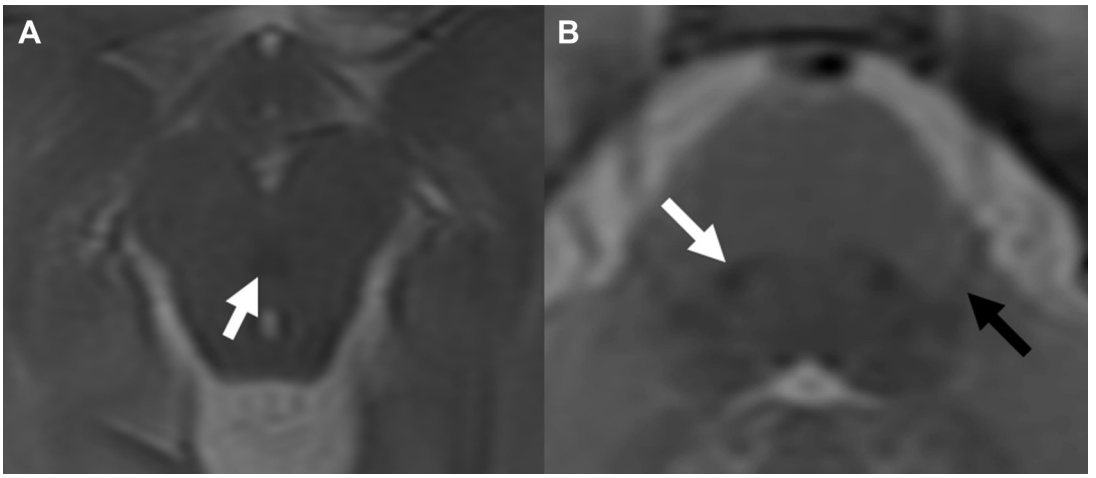

Fig. 3. (*A*) Axial T2-weighted image through the midbrain in a 5-week-old girl born at 25 weeks' gestation (corrected gestational age 30 weeks) demonstrates hypointensity in the region of CN III.a (*arrow*). (*B*) In the same patient, at the level of the pons, CN VII.a (*white arrow*) and a component of CN V.b (*black arrow*) are noted.

imaging, because the tightly packed layers of mature myelin around the nerve fibers have a decreased water content compared with the surrounding incompletely myelinated parenchyma.[21] The fascicles are not typically visualized on standard anatomic imaging in patients who are maturely myelinated but may be outlined by pathologic conditions. In the research realm, advances in high-resolution imaging shows promise for more clear depiction of the fascicular segments at higher field strengths than those currently used clinically.[26] Likewise, the root exit point and AS are not readily appreciated on modern clinical imaging and must be inferred by comparison to anatomic references.

Diffusion tensor imaging DTI is a technique that allows identification of fiber tracts within the brain parenchyma by virtue of the manner in which they constrain water diffusion. The technique has been used with limited success for visualization of the CN fascicles, largely due to their small size. The tracts associated with CN II and CN III.b are visualized with success.[27] In one patient with CN III palsy, abnormal signal in the region of CN III.b not well seen on standard imaging was demonstrated with thin-section DTI.[28] In the research setting, multishot diffusion-weighted imaging with periodically rotated overlapping parallel lines with enhanced reconstruction (PROPELLER) has been suggested to improve visualization of the visualization of the fascicular component of the CNs in normal volunteers but with insufficient signal-to-noise ratio for routine clinical use.[29]

Selected pathologic entities

The fascicular segment of the CNs may be interrupted by any pathologic condition within the brainstem, including demyelinating disease and neoplastic processes, such as those arising from the glial support cells found in the CNS or other masses. Surgical data on patients treated for hemifacial spasm suggest that the neurovascular compression occurs in the terminal fascicular component of the CN VII.b in many cases, often with compression of the brainstem rather than the cisternal segment itself as generally assumed[24] (discussed later).

c. Cisternal Segment

Anatomic considerations

The end of the parenchymal fascicular segment and beginning of the cisternal segment is known anatomically as the root detachment point,[23,24] corresponding approximately to the AO, where the CN can be visualized surrounded by CSF on imaging (**Fig. 4**B). As described previously, the root exit point is not synonymous with the AO for at least some of the CNs. The term, *root exit zone*, is considered ambiguous[23] and its use is discouraged. Occasionally, multiple small free rootlets are visible (see **Fig. 4**) that converge on a root or several individual roots.[25,30,31]

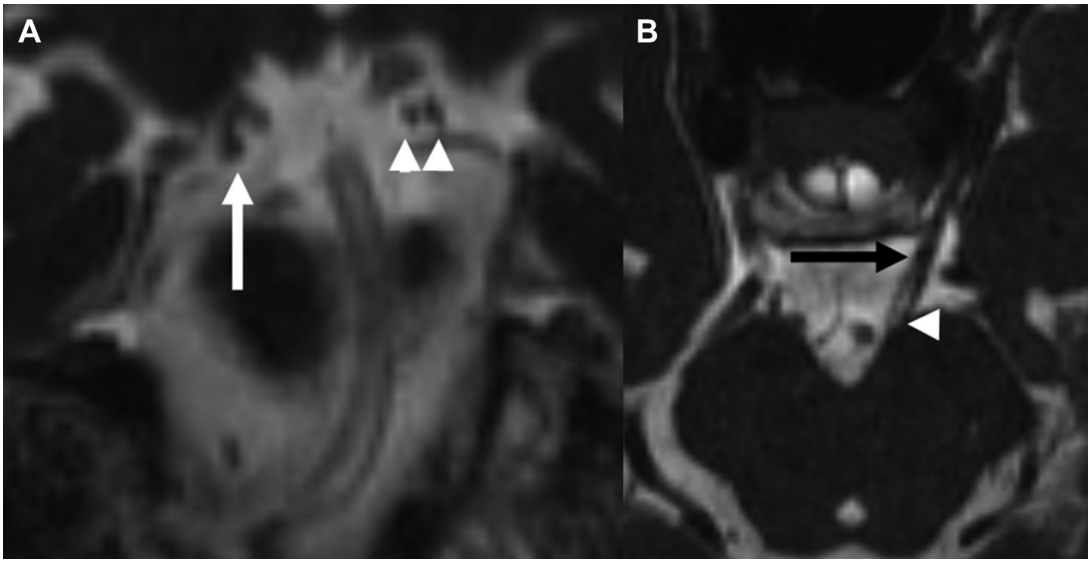

Fig. 4. (*A*) Coronal reformatted CISS demonstrates 2 rootlets of the proximal left CN III.c (*arrowheads*). Typical anatomy with a single root of CN III.c is seen on the right (*arrow*). (*B*) Axial CISS demonstrates the proximal rootlets joining (*arrow*) to form a single left CN III.c root within the midcisternal segment. The point of AO of the left CN III.c is marked with an arrowhead.

The proximal nerves in this segment are covered by pia mater[32] and surrounded by CSF within the subarachnoid space. In the cisternal segment, the CNs may adjoin arterial or venous structures as well as the arachnoidal septae. Arterial or venous structures may directly abut, surround, or even divide the cisternal components of the CNs.[33] The cisternal nerve roots extend toward the porus of the dural cave segment (described later) (**Fig. 5**).

The zone of transition between the oligodendrocyte-myelinated CNS and the Schwann cell–myelinated PNS is called the CNS-PNS transitional zone (TZ) (sometimes given the eponym Obersteiner-Redlich zone). The TZ was initially described as a thinning of the myelin sheaths of spinal nerves just before the junction of the dorsal root and the cord,[34] and the CNS component of the nerve proximal to this point is thought more prone to irritation. This point of transition is visible to the neurosurgeon through the operating microscope, because pia mater can be seen covering the centrally myelinated CNS component.[32]

The length of the centrally myelinated portion of the cisternal segment and, therefore, the site of the TZ varies between the CNs. Among CNs III–XII (as reported by Lang[32]) the TZ is approximately 1 mm or less from the AO at the surface of the brainstem for CNs IV, V (motor root only), VI, IX, X, and XI. The other CNs vary significantly in the length of the CNS component/location of the TZ. The TZ of CN III.c is typically located 1.9 mm (range 1.0–4.0 mm) from the AO; the TZ of CN VII.c is located 2.1 mm (range 0.5–4.0 mm) from the AO; the TZ for the sensory root of CN V.c is located on average 3.6 mm (range 2.0–6.0 mm) from the AO. The longest centrally myelinated cisternal component of a CN is that of CN VIII.c, with the TZ located most often at or near the porus acousticus, approximately 10.0 mm from the brainstem (range 6.0–15.0 mm).[32]

Imaging approaches

CN evaluation in the cisternal segment most often depends on negative contrast with a heavily T2-weighted appearance of CSF, an approach sometimes termed, *magnetic resonance cisternography*.

Although the cisternal CNs are generally well visualized, reports of visualization of CN IV.c have been variously reported as inconsistent[35] to excellent,[9] depending on technique and owing to its small size. Visualization is significantly improved with voxel sizes less than the diameter of the nerve.[9] The site of the TZ, although visible to neurosurgeons through the operating microscope,[32] is not readily identifiable through imaging alone, and its approximate location must be inferred through knowledge of the relevant CN anatomy.

Spin-echo T2-weighted imaging Early MR imaging experience with imaging of the cisternal CNs with 2-D heavily T2-weighted turbo spin-echo imaging using peripheral pulse gating to minimize CSF flow artifacts was successful, particularly in visualizing CNs I, II, III, VII, and VIII.[36] Subsequent studies demonstrated a significant advantage in detection of the CNs with 3-D compared with 2-D fast spin-echo sequences.[13] The addition of driven equilibrium radiofrequency reset pulse (DRIVE) to turbo spin-echo 3-D imaging has been shown to reduce CSF flow artifacts with lower scan times.[37] Comparison of 3-D fast asymmetric spin-echo and 3-D CISS imaging of the cerebellopontine angle cistern by one group of investigators

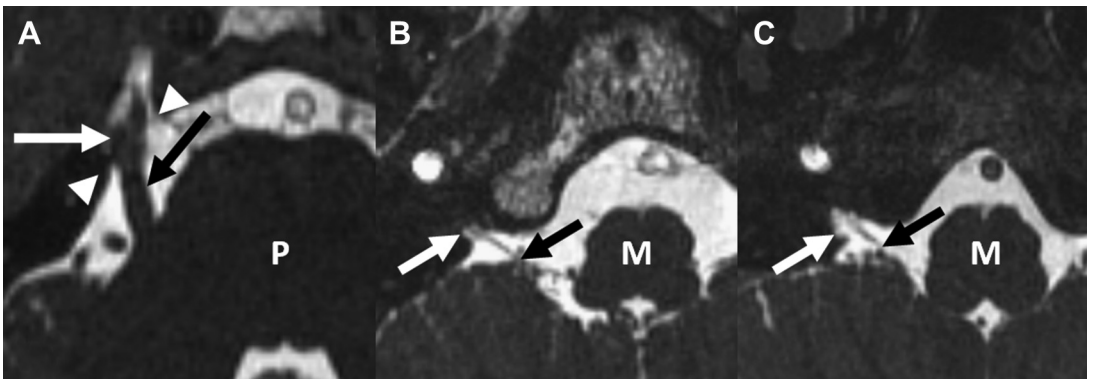

Fig. 5. (*A*) Axial CISS image demonstrates CN V.c (*black arrow*) as a filling defect surrounded by T2 hyperintensity of CSF within the subarachnoid space extending from the pons (P) through the porus trigeminus (*arrowheads*) to enter the trigeminal cistern within the Meckel cave as CN V.d (*white arrow*). (*B*) At the level of the medulla (M) CN IX.c (*black arrow*) extends through the jugular porus into a small dural cave (*white arrow*) of the right jugular foramen on precontrast CISS. (*C*) Significant variation is seen from patient to patient in the size of the dural cave segment; compare the extent of CSF evagination to that seen in (*B*).

favored 3-D fast asymmetric spin-echo due to "more prominent flow ghosts and magnetic susceptibility artifacts" on CISS.[38]

Steady-state free precession imaging High-resolution steady-state free precession (SSFP) sequences with a heavily T2-weighted appearance have become the mainstay of visualization of the cisternal component of the CNs[39] since their introduction by Casselman and colleagues.[40] Several studies have assessed visualization of the CNs in the cisternal segment.[35,41] 3-D CISS[11,35] and the analogous 3-D fast imaging using steady-state acquisition (FIESTA)[12] have been shown to be superior to 2-D T2-weighted images for the cisternal CNs. Additionally, comparison of CISS to 3-D magnetization-prepared rapid gradient echo (MP-RAGE), a T1-weighted 3-D technique, has favored CISS.[11] In patients undergoing surgery for neurovascular compression of CN V.c, comparison of CISS to magnetic resonance angiography (MRA) suggested that CISS more accurately predicts intraoperative findings with respect to the relationship of vascular structures to the CN.[42]

Although commonly thought of as a T2-weighted technique, CISS and FIESTA-C are fully refocused (balanced) steady-state sequences that demonstrate both T2 and T1 components.[43] This combination of weightings is ideal for the evaluation of the CNs because it allows both high spatial resolution with suppression of CSF flow artifacts and the use of contrast agents (Fig. 6). The use of contrast-enhanced CISS images for evaluation of cisternal masses has been proposed by Shigematsu and colleagues,[44] who suggested that the technique could reveal the accurate location of CN VII.c and CN VIII.c relative to cerebellopontine angle masses.

Diffusion tensor imaging Hodaie and colleagues[27] assessed visualization of the CNs, finding that evaluation of the lower cisternal CNs was particularly challenging. DTI has been used to determine the location of CN VII.c and CN VIII.c adjacent to large vestibular schwannomas in the cerebellopontine angle cistern.[45,46] In addition to information on the location of the cisternal components of the CNs, DTI reveals alterations in the coherence of water diffusion (fractional anisotropy) and has been shown to demonstrate significantly decreased fractional anisotropy in CN V.c on the side affected by trigeminal neuralgia[47] due to neurovascular compression.

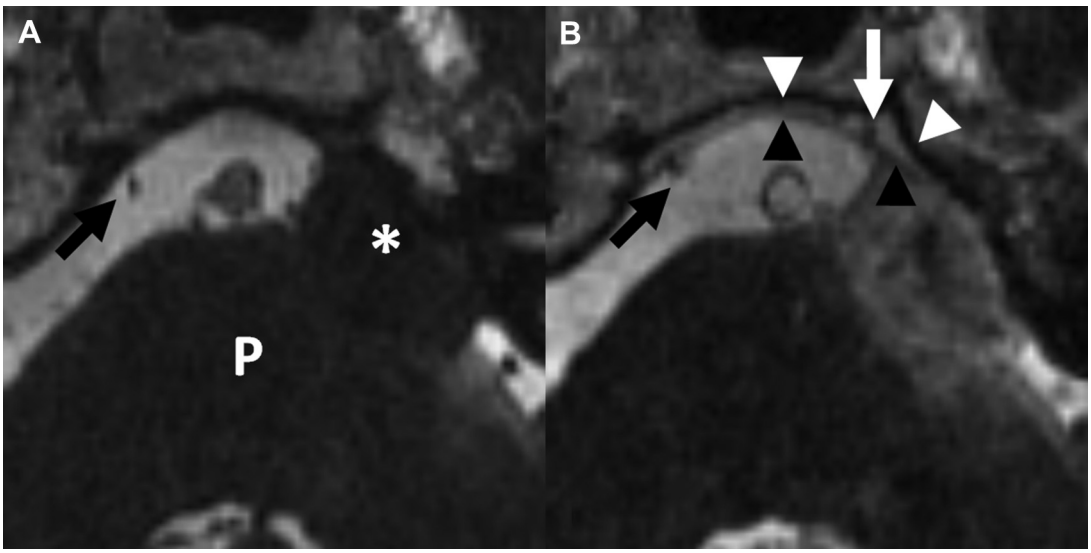

Fig. 6. (*A*) On axial precontrast CISS, the right CN VI.c (*black arrow*) is noted. A mass (*asterisk*) fills the left prepontine cistern indenting the left ventral pons (P). The location of the left CN VI.c is ambiguous. (*B*) After the administration of intravenous contrast, the left CN VI.e (*white arrow*) is clearly seen in the petroclival venous confluence. As seen in the precontrast image, right CN VI.c (*black arrow*) has not yet pierced the dura at this level, reflecting slight physiologic asymmetry in the cranial-caudal location of CN VI.d. The relationship of the mass to the inner layer of dura (*black arrowheads*) is now clear, without evidence of extension of the presumed meningioma into the interdural space adjacent to CN VI.e. The inner table of the skull (*white arrowheads*) to which the outer periostial layer of dura is applied, denoting the outer margin of the interdural space, is also noted. The patient presented with left-sided facial pain and decreased facial sensation due to compression of the left CN V.c (not shown). Extraocular movements were intact.

Selected pathologic entities

There are several clinical implications of the location of the TZ within the cisternal segment for most of the CNs. CN injuries distal to the TZ (ie, within the PNS) have different clinical implications from proximal CNS injuries. The PNS may regenerate with near-normal function, unlike the CNS, where a gliotic response to injury and persistent loss of axons is normal.[48] Because glial cells differ between the CNS and PNS pathology, the TZ forms a boundary for differential diagnostic considerations as well. Because Schwann cells are found only in the PNS, schwannomas likewise are found only distal to the TZ. In cases of vestibular schwannomas, for instance,[49] because the TZ for CN VIII is often found at or near the porus acousticus, the diagnosis of vestibular schwannoma is unlikely for masses located within the cerebellopontine angle cistern without involvement of the internal auditory canal.

The basal cisterns contain numerous arterial and venous structures. Since it was first demonstrated by Janetta[50] that neurovascular compression could cause trigeminal neuralgia and that neurosurgical decompression could result in relief from pain, several similar syndromes of neurovascular conflict have been identified. In these syndromes, grouped together as the hyperactive dysfunctional syndromes, irritation or injury to the cisternal segment of the CNs from direct contact with vascular structures is hypothesized. Although hyperactive dysfunctional syndromes may arise due to compression of any segment of a CN, the centrally myelinated components of the nerve are more vulnerable to such syndromes. In particular, trigeminal neuralgia, hemifacial spasm, and vagoglossopharyngeal neuralgia have been associated with neurovascular compression of CN V.c, CN VII.c, and CN IX/CN X.c, respectively. The susceptibility of these nerves to neurovascular compression is thought proportionate to the length of the centrally myelinated component within the cistern.[51]

Readers should be aware that neurovascular contact is common in the absence of the symptoms discussed previously. One study found neurovascular contact with CN V.c is seen in 49% and CN VII.c in 79% of asymptomatic individuals.[52] Additionally, a surgical series of microvascular decompression of CN VII for hemifacial spasm demonstrated compression in the 74% of cases not in CN VII.c but rather the attached segment distal segment of CN VII.b.[24] Although imaging may predict the intraoperative findings in many patients,[42] false-negative and false-positive cases are common.[53] As discussed previously, the measurement of fractional anisotropy with DTI has been reported as abnormal in trigeminal neuralgia and may increase specificity when neurovascular compression of CN V.c is suspected.[47] Such an approach is less likely to be helpful for CNs of smaller diameter due to spatial resolution and current system limitations.

d. Dural Cave Segment

Anatomic considerations

As the CNs leave the intracranial compartment, they transit several complex anatomic spaces. The dural cave segment is surrounded by an evagination of the arachnoid membrane within the inner (variously known as the lamina propria, cerebral, or meningeal) layer of the dura and its opening is called the porus (see **Fig. 5**). The dural cave forms the region of transition from the cisternal segment centrally to the interdural segment distally. The segment is variable from CN to CN and may also vary in prominence from individual to individual (see **Fig. 5**). In this regard, CN V.d that resides within the Meckel cave is the most familiar and provides an archetype of the relevant anatomic considerations. Each of the CNs makes a similar transition, with the dural cave of CN VI, for instance, also formed by an evagination of the inner layer of dura lined by arachnoid membrane.[54]

Generically, the location where the nerve passes out of the subarachnoid space and is no longer surrounded by CSF is termed, *the subarachnoid angle*.[55] For CN V.d, the arachnoid membrane typically terminates as perineurium distal to the posterior margin of the gasserian ganglion.[56] The point at which the arachnoid becomes adherent to the ganglion and its distal divisions is variable, however; thus, the volume and extent of the trigeminal cistern are variable. Although this cistern closely approximates the dimensions of the Meckel cave, and for the purposes of imaging is defined as the region with visible CSF surrounding the CN V, the two are not formally synonymous, with the Meckel cave slightly larger and extending farther anteriorly than the trigeminal cistern proper.[57]

Imaging approaches

Spin-echo–based T2-weighted imaging The use of 3-D fast asymmetric spin-echo magnetic resonance has been described for evaluation of CN VI.d (although not described as such) in volunteers.[58]

Steady-state free precession imaging CSF within the dural caves is well visualized with high-resolution T2-weighted SSFP imaging. The use of noncontrast CISS imaging for evaluation of CN III.d[59] as well as CN VI.d[60] have been described. Yousry and colleagues[61] also reported the use of

postcontrast CISS for visualization of the gasserian (trigeminal) ganglion within the Meckel cave.

Selected pathologic entities

Although dural-based masses, such as meningioma, may become sufficiently large to compress a CN anywhere in the cisternal segment, small masses may become symptomatic at an earlier point if strategically positioned within the region of the dural interface (**Fig. 7**). Schwannoma may affect the CNs at any point distal to the TZ but seems to predilect the dural cave segment.

e. Interdural Segment

Anatomic considerations

The dura mater is composed of two layers.[56] The outer (periosteal) layer is closely adherent to the underlying bone and is continuous with the outer periosteum of the skull through sutures and neural foramina. The inner layer of dura (also known as lamina propria or meningeal or cerebral layer) is typically fused with the outer dural layer. There are interdural spaces, however, where the two are not closely opposed, such as in the region of the dural venous sinuses,[62] and the space between the inner and outer layers of dura contains an extensive venous plexus.[63] Several of the CNs exit the inner layer of dura and course between the inner and outer dural layers in the interdural compartment[64] before exiting the cranial vault through the skull base foramina. The prototypical space in this regard is the cavernous sinus, in which CNs III.e, IV.e, V.1.e, V.2.e and VI.e are surrounded by venous blood.

Imaging approaches

Postcontrast SSFP Although high-resolution 3-D imaging has traditionally principally been used without contrast for the evaluation of the cisternal segments of the CNs (described previously), administration of contrast and use of mixed-weighting SSFP or reversed fast imaging with steady-state precession (PSIF) (described later) sequences allows simultaneous high spatial resolution and evaluation of contrast enhancement. For this reason, the CNs, which do not normally enhance, can be well visualized inside the cavernous sinuses surrounded by contrast-enhanced venous blood (**Fig. 8**).[65] The petroclival CN VI.e is also well seen on CISS after the administration of intravenous contrast (see, for instance, **Fig. 6**B and the accompanying article by Blitz and colleagues in this issue).

Contrast-enhanced magnetic resonance angiography Linn and colleagues[66] described the application of contrast-enhanced MRA (CE-MRA) for evaluation of the cavernous segments of the CNs. Much like the approach taken with postcontrast CISS, CE-MRA relies on contrast enhancement of the venous plexus surrounding the cavernous CNs. The authors used a CE-MRA technique on a 3-T MR imaging lasting greater than 7 minutes' duration. The authors were able to produce multiplanar reconstructed images that depict the cavernous segments of the CNs in relation to sellar and cavernous masses extremely well.

Selected pathologic entities

The interdural space sits at the intersection of the osseous structures of the skull base and the intracranial compartment. Neoplastic processes arising from the meninges (see **Fig. 6**) or nerve root sheaths as well as inflammatory processes

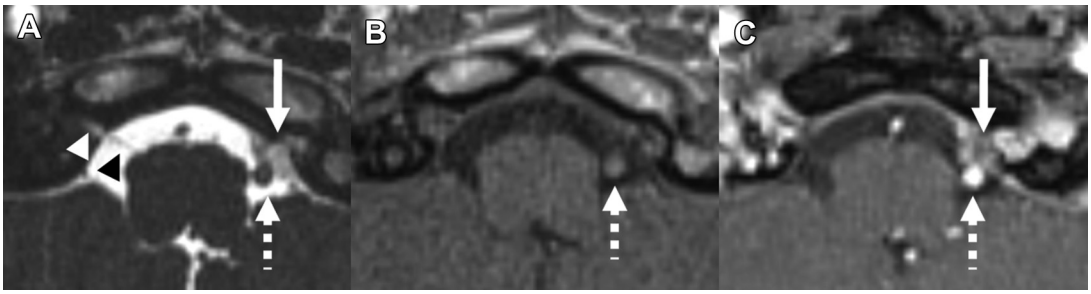

Fig. 7. A 57-year-old woman presented with denervation of her left tongue of uncertain cause. Standard MR imaging had been unrevealing. (*A*) Axial noncontrast CISS demonstrates the right CN XII.c (*black arrowhead*) extending toward a small dural cave (*white arrowhead*, continued for reference in following frames). On the left side an approximately 6 mm mass (*white arrow*) is noted extending from the region of the left CN XII.d into the cistern just anterolateral to the V4 segment of the left vertebral artery (*dashed arrow*). The mass was not visualized on noncontrast axial volumetric interpolated breath-hold examination (VIBE), a T1-weighted technique. (Please note that breath holds are not typically employed with this technique when employed in neuroradiology despite the acronymn.) (*B*) but demonstrated enhancement (*white arrow*) on postcontrast fat saturated VIBE (*C*).

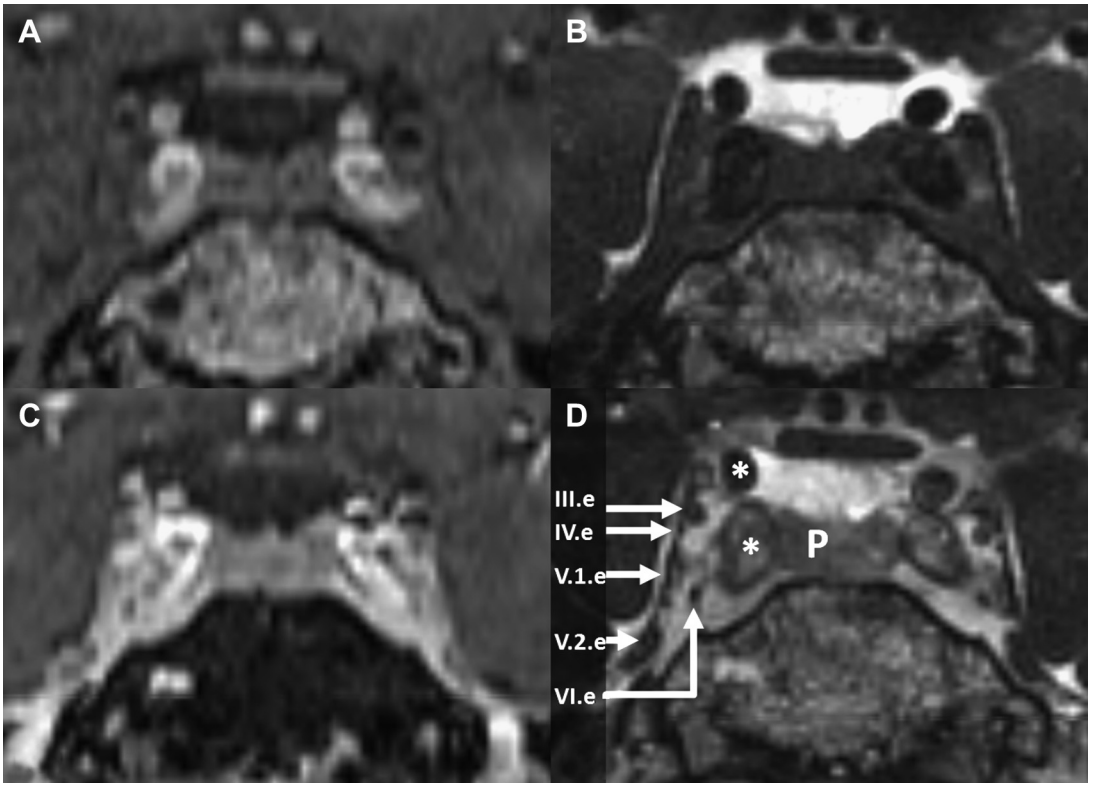

Fig. 8. Coronal reformatted images through the level of the cavernous sinus. (*A*) Precontrast VIBE. (*B*) Precontrast CISS. (*C*) Postcontrast VIBE demonstrates enhancement of the cavernous sinus. (*D*) Postcontrast CISS best demonstrates the normal appearance of the interdural oculomotor (III.e), trochlear (IV.e), ophthalmic (V.1.e), maxillary (V.2.e), and abducens (VI.e) nerves. The internal carotid artery (*asterisk*) and pituitary (P) are labeled for orientation purposes.

may be seen in this region. Additionally, intraosseous abnormalities may gain access to the interdural space if they pierce the outer layer of dura. Perineural spread of disease passing intracranially through the foraminal regions may also affect the interdural space. Pituitary region pathologies likewise may spread into the interdural space, in particular, the cavernous sinus.

f. Foraminal Segment

Anatomic considerations

The passage of the CNs through the skull is accomplished via the skull base foramina. The foraminal segment of each CN is defined as extending from the inner margin of the internal orifice of the foramen through the outer margin of the outer table of the skull at the external orifice. CN VIII alone among the CNs does not have a component that exits the skull base. The foramina are lined by the outer (periostial) layer of dura, which is continuous at the outer margin of the foramina with the periosteum as well as the epineurium.[56] The CNs are typically surrounded in their foraminal segments by a circumneural venous plexus, the enhancement of which allows visualization of the normally nonenhancing CN.[14]

Imaging approaches

Evaluation of the osseous margins of the skull base foramina is most frequently accomplished clinically with CT; however, MR imaging has the added advantage of allowing visualization of the CN with contrast-enhanced technique (**Fig. 9**A, B). Just as contrast-enhanced venous blood allows visualization of the CNs in the cavernous sinus, the presence of cortical bones lining the skull base foramina and venous plexus surrounding the foraminal components of the CNs allows similar high-resolution 3-D evaluation on postcontrast sequences. The jugular foramen, given its complexity, is an excellent example of the potential visualization of the CNs as they pass through the foraminal segment.

Postcontrast SSFP After the administration of intravenous contrast, CN IX.f, CN X.f, and CN XI.f are well visualized within the jugular foramen due to surrounding venous enhancement on FIESTA.[67]

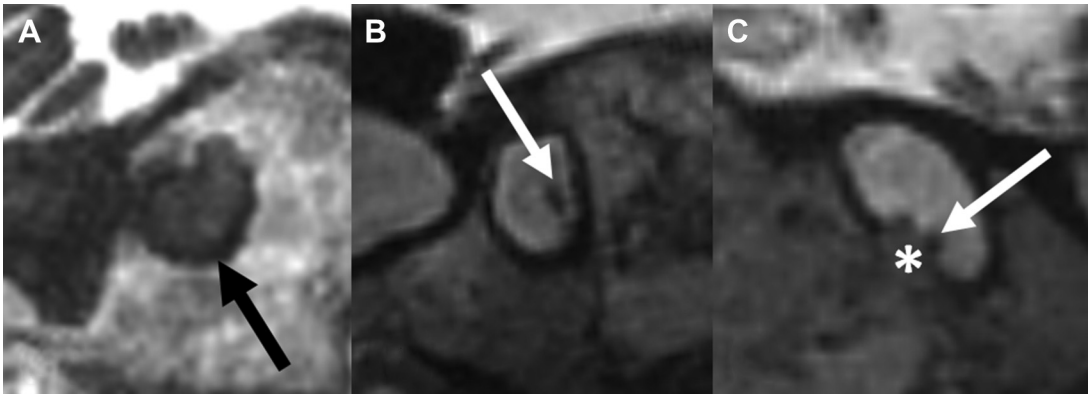

Fig. 9. (*A*) Precontrast CISS in a patient without osseous pathology of the skull base. Multiplanar reformat perpendicular to the hypoglossal canal demonstrating the cortical margin (*arrow*). (*B*) Postcontrast CISS demonstrates CN XII.f (*arrow*) surrounded by enhancement of the venous plexus. The cortical margin of the foramen is intact. (*C*) On the contralateral side, a component of a large chordoma (*asterisk*) involving the posterior skull base interrupts the cortical margin of the foramen and minimally extends into the hypoglossal canal to abut CN XII.f (*arrow*).

Contrast-enhanced magnetic resonance angiograph Linn and colleagues[68] have described the use of CE-MRA in the jugular foramen and reported overall improved visualization of the CNs compared with contrast-enhanced FIESTA although some structures were better visualized with contrast-enhanced FIESTA. The investigators were careful to match time of acquisition; however, CE-MRA was performed before contrast-enhanced FIESTA. It is not clear to what extent the greater than 7-minute delay for performance of CE-MRA may have had on comparison with the subsequently performed FIESTA. The investigators suggest performance of CE-MRA if pathology of the foramen itself is suspected and FIESTA imaging for cases when lower CN pathology is suspected but the timing is less clear.

Selected pathologic entities

When encountered in isolation, pathologic conditions of the foraminal segment of the CNs are most commonly the result of extension of an abnormality from within the adjacent bone (eg, see **Fig. 9**C).

g. Extraforaminal Segment

Anatomic considerations

The extraforaminal segment (g) begins at the plane that passes through the outer cortex of the outer margin of the appropriate foramen. The proximal extraforaminal segment typically passes at least initially through fat before coming into contact with the vascular structures, glands, and muscles of the head and neck. Among the CNs, CN X.g has the most extensive extraforaminal course (implied by the name of CN X, *vagus* [wanderer]) and reaches as far as the abdomen.

Imaging approaches

CISS with and without contrast Both fat and fluid return high signal on balanced SSFP sequences, such as CISS, due to their high T2/T1 ratios.[43] The environment of the extraforaminal CNs consists of fat, muscle, bone, and vascular structures, which can be readily distinguished on CISS. Despite the course of multiple extraforaminal components of the CNs near the air-containing paranasal sinuses and aerodigestive tract, perhaps because of the reduced T2* sensitivity of balanced SSFP sequences[43] as well as the small voxels used, resultant artifacts tend not to significantly limit such evaluations. The use of CISS imaging in the extraforaminal regions of the suprahyoid neck allows exquisite anatomic definition of structures that have not been typically well visualized with prior techniques (**Fig. 10**) and has been extensively used at the authors' institution for this purpose. The addition of intravenous contrast heightens the distinction between the extraforaminal CNs and adjacent structures. In conjunction with 3-D T1 and short tau inversion recovery (STIR) sequences, comparison of precontrast and postcontrast CISS imaging allows evaluation of small regions of pathologic enhancement, such as might be encountered in perineural spread of neoplasm or in highlighting the relationship of the CN to an enhancing mass (see **Fig. 10**C).

Reverse FISP/Neurography 3-D PSIF with diffusion weighting has been reported by Zhang and colleagues[69] as demonstrating the course of the CNs. The investigators evaluated the results of an approximately 10-minute PSIF acquisition with a diffusion moment of 20 mT/m*ms and concluded the technique "cannot be used as a

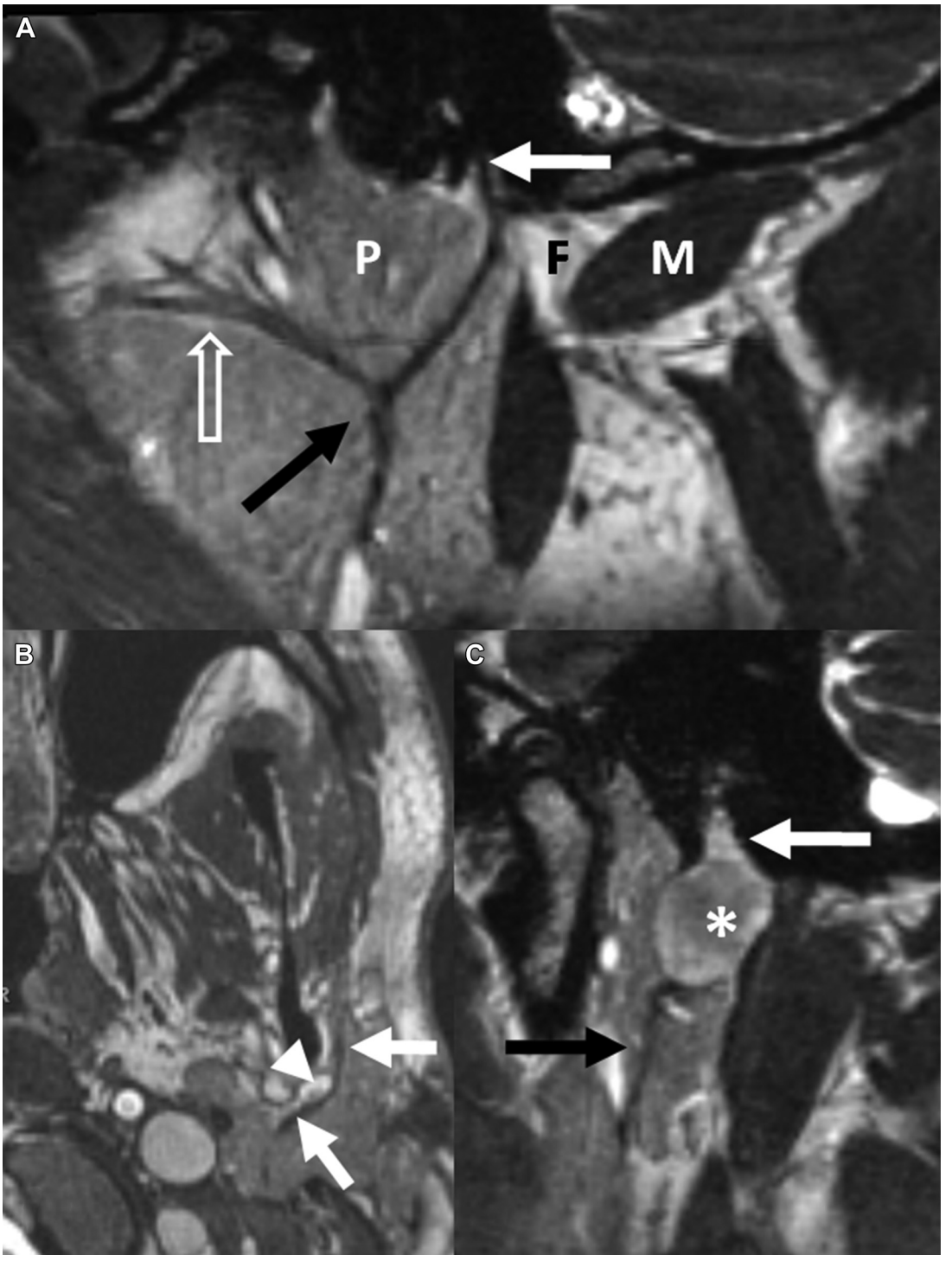

Fig. 10. (*A*) Sagittal oblique postcontrast CISS through the region of the parotid. CN VII.g is seen exiting the stylomastoid foramen (*white closed arrow*) and coursing inferiorly to enter the parotid gland (P). The primary intraparotid branch point (*black arrow*) into the temporofacial branch (superiorly) and cervicofacial branch (inferiorly) are seen. Secondary (*open white arrow*) intraparotid branch points are also well visualized as the nerve extends anteriorly. High-resolution imaging of the CNs in the extraforaminal compartment relies on differential signal characteristics of the CNs surrounded by fat (F), muscle (M), and organs, such as the parotid (P). (*B*) Axial postcontrast CISS demonstrates the relationship of the intraparotid CN VII.g (*arrows*) to the retromandibular vein (*arrowhead*). (*C*) Sagittal postcontrast CISS in a different patient demonstrates an enhancing mass (*asterisk*) extending from the stylomastoid foramen (*white arrow*) into the parotid gland. The distal intraparotid CN VII.g (*black arrow*) can be seen emanating from the caudal aspect of the mass, a presumed schwannoma.

substitute for other standard sequences such as 3D-CISS sequence or the 3-D fast spin echo (FSE) sequence" but may be most useful for evaluation of CNs outside of the cranial compartment. This technique may be most useful in regions, such as the carotid sheath, where visualization of the CNs is inconstant.

Diffusion tensor imaging DTI using fat saturation at 3T with tractography has been reported by Akter and colleagues[70] for imaging of the CNs within the head and neck; they describe at least partial correlation between DTI and operative findings in 4 of the 5 patients studied.

SUMMARY

Imaging of the CNs presents a challenge due to their small size and course. This article proposes a segmental classification system for radiologic evaluation of the CNs, which the authors hope proves useful in clinical practice while providing a framework for future high-resolution CN imaging research. MR imaging is currently the gold standard technique and a variety of pulse sequences are available to demonstrate the CNs. The optimal imaging approach depends largely on which sequence is best suited to demonstrating the CN in the segment of interest. Within the nuclear and fascicular segments, the CNs are often difficult to distinguish from surrounding brain parenchyma. Cisternal and dural cave segments are best visualized on T2-weighted sequences and SSFP sequences. The interdural segments are best seen with techniques that allow enhancement of the surrounding venous blood, such as contrast-enhanced MRA or contrast-enhanced SSFP sequences; a similar approach is helpful for visualization within the skull base foramina. Within the extraforaminal segment, the CNs adjoin vascular structures, fat, muscle, and/or bone as they pass through the head and neck and may be visualized with a variety of techniques with SSFP sequences, such as CISS and PSIF, providing excellent anatomic detail. DTI has also been used for visualization of the CNs in the fascicular, cisternal, and extraforaminal segments.

The heterogeneity of anatomic context presents significant challenges for images. Given advantages and pitfalls of various imaging pulse sequences, a fully refocused SSFP technique, such as CISS, allows visualization of much of the CN course when precontrast and postcontrast techniques are used. The accompanying article by Blitz and colleagues elsewhere in this issue describes the relevant anatomy and imaging appearance of the upper CNs on high-resolution CISS imaging, using the segmental approach advocated in this article.

REFERENCES

1. Brazis PW, Masdeu JC, Biller J. Localization in Clinical Neurology. Philadelphia: Lippincott Williams & Wilkins; 2011.
2. Di Chiro G. An Atlas of Detailed Normal Pneumoencephalographic Anatomy, 2e. Springfield: Charles C. Thomas Publisher; 1971.
3. de Slegte R, Valk J, Lohman A, et al. Cisternographic Anatomy of the Poster Cranial Fossa: High Resolution CT and MRI Study. Wolfeboro: Vam Gorcum; 1986.
4. Fischbach F, Müller M, Bruhn H. Magnetic resonance imaging of the cranial nerves in the posterior fossa: a comparative study of t2-weighted spin-echo sequences at 1.5 and 3.0 tesla. Acta Radiol 2008;49(3):358–63.
5. Penn R, Abemayor E, Nabili V, et al. Perineural invasion detected by high-field 3.0-T magnetic resonance imaging. Am J Otolaryngol 2010;31(6): 482–4.
6. Hart H, Bottomley P, Edelstein W, et al. Nuclear magnetic resonance imaging: contrast-to-noise ratio as a function of strength of magnetic field. Am J Roentgenol 1983;141(6):1195–201.
7. Casselman J, Mermuys K, Delanote J, et al. MRI of the cranial nerves—more than meets the eye: technical considerations and advanced anatomy. Neuroimaging Clin N Am 2008;18(2):197–231.
8. Fischbach F, Müller M, Bruhn H. High-resolution depiction of the cranial nerves in the posterior fossa (N III–N XII) with 2D fast spin echo and 3D gradient echo sequences at 3.0 T. Clin Imaging 2009;33(3):169–74.
9. Choi B, Kim J, Jung C, et al. High-resolution 3D MR imaging of the trochlear nerve. AJNR Am J Neuroradiol 2010;31(6):1076–9.
10. Leblanc A. The Cranial Nerves: Anatomy, Imaging, Vascularisation. New York: Springer-Verlag; 1995.
11. Held P, Nitz W, Seitz J, et al. Comparison of 2D and 3D MRI of the optic and oculomotor nerve anatomy. Clin Imaging 2000;24(6):337–43.
12. Hatipoğlu HG, Durakoğlugil T, Ciliz D, et al. Comparison of FSE T2W and 3D FIESTA sequences in the evaluation of posterior fossa cranial nerves with MR cisternography. Diagn Interv Radiol 2007;13(2):56–60.
13. Iwayama E, Naganawa S, Ito T, et al. High-resolution MR cisternography of the cerebellopontine angle: 2D versus 3D fast spin-echo sequences. AJNR Am J Neuroradiol 1999;20(5):889–95.
14. Williams LS, Schmalfuss IM, Sistrom CL, et al. MR imaging of the trigeminal ganglion, nerve, and the perineural vascular plexus: normal appearance

and variants with correlation to cadaver specimens. AJNR Am J Neuroradiol 2003;24(7):1317–23.
15. Gebarski S, Telian S, Niparko J. Enhancement along the normal facial nerve in the facial canal: MR imaging and anatomic correlation. Radiology 1992;183(2):391–4.
16. Saremi F, Helmy M, Farzin S, et al. MRI of cranial nerve enhancement. Am J Roentgenol 2005; 185(6):1487–97.
17. Whitmore I. Terminologia Anatomica: International Anatomical terminology; FIPAT, Federative international Programme on Anatomical Terminologies. New York: Thieme; 2011.
18. Nieuwenhuys R, Voogd J, Voogd J, et al. The Human Central Nervous System, 4e. Springer Verlag; 2008.
19. Wilson-Pauwels L, Akesson EJ, Stewart PA. Cranial Nerves. Hamilton, Canada: Decker; 1988.
20. Nolte J. The Human Brain: An Introduction to its Functional Anatomy, 5e. St. Louis: Mosby; 2002.
21. Barkovich AJ. MR of the normal neonatal brain: assessment of deep structures. AJNR Am J Neuroradiol 1998;19(8):1397–403.
22. Nagae-Poetscher LM, Jiang H, Wakana S, et al. High-resolution diffusion tensor imaging of the brain stem at 3 T. AJNR Am J Neuroradiol 2004; 25(8):1325–30.
23. Tomii M, Onoue H, Yasue M, et al. Microscopic measurement of the facial nerve root exit zone from central glial myelin to peripheral Schwann cell myelin. J Neurosurg 2003;99(1):121–4.
24. Campos-Benitez M, Kaufmann AM. Neurovascular compression findings in hemifacial spasm. J Neurosurg 2008;109(3):416–20.
25. Fraher J, Smiddy P, O'Sullivan V. The central-peripheral transitional regions of cranial nerves. Oculomotor nerve. J Anat 1988;161:103–13.
26. Naidich TP, Duvernoy HM, Delman BN, et al. Duvernoy's Atlas of the Human Brain Stem and Cerebellum. Vienna (Austria): Springer-Verlag; 2009.
27. Hodaie M, Quan J, Chen DQ. In vivo visualization of cranial nerve pathways in humans using diffusion-based tractography. Neurosurgery 2010;66(4): 788–96.
28. Yamada K, Shiga K, Kizu O, et al. Oculomotor nerve palsy evaluated by diffusion-tensor tractography. Neuroradiology 2006;48(6):434–7.
29. Adachi M, Kabasawa H, Kawaguchi E. Depiction of the cranial nerves within the brain stem with use of PROPELLER multishot diffusion-weighted imaging. AJNR Am J Neuroradiol 2008;29(5):911–2.
30. Nathan H, Ouaknine G, Kosary IZ. The abducens nerve. J Neurosurg 1974;41(5):561–6.
31. Fraher J, Smiddy P, O'Sullivan V. The central-peripheral transitional regions of cranial nerves. Trochlear and abducent nerves. J Anat 1988;161: 115–23.
32. Lang J. Clinical Anatomy of the Head. Berlin: Springer-Verlag; 1983.
33. Marinkovic SV, Gibo H, Stimec B. The neurovascular relationships and the blood supply of the abducent nerve: surgical anatomy of its cisternal segment. Neurosurgery 1994;34(6):1017–26.
34. Obersteiner H, Redlich E. Ueber Wesen Und Pathogenese Der Tabischen Hinterstrangsdegeneration. Arb Neurol Inst Univ Wien 1894;1(3):152–72.
35. Yousry I, Camelio S, Schmid U, et al. Visualization of cranial nerves I–XII: value of 3D CISS and T2-weighted FSE sequences. Eur Radiol 2000; 10(7):1061–7.
36. Mamata Y, Muro I, Matsumae M, et al. Magnetic resonance cisternography for visualization of intracisternal fine structures. J Neurosurg 1998;88(4): 670–8.
37. Ciftci E, Anik Y, Arslan A, et al. Driven equilibrium (drive) MR imaging of the cranial nerves V–VIII: comparison with the T2-weighted 3D TSE sequence. Eur J Radiol 2004;51(3):234–40.
38. Naganawa S, Koshikawa T, Fukatsu H, et al. MR cisternography of the cerebellopontine angle: comparison of three-dimensional fast asymmetrical spin-echo and three-dimensional constructive interference in the steady-state sequences. AJNR Am J Neuroradiol 2001;22(6):1179–85.
39. Sheth S, Branstetter BF IV, Escott EJ. Appearance of normal cranial nerves on steady-state free precession MR images1. Radiographics 2009;29(4): 1045–55.
40. Casselman J, Kuhweide R, Deimling M, et al. Constructive interference in steady state-3DFT MR imaging of the inner ear and cerebellopontine angle. AJNR Am J Neuroradiol 1993;14(1):47–57.
41. Seitz J, Held P, Fründ R, et al. Visualization of the IXth to XIIth cranial nerves using 3-dimensional constructive interference in steady state, 3-dimensional magnetization-prepared rapid gradient echo and T2-weighted 2-dimensional turbo spin echo magnetic resonance imaging sequences. J Neuroimaging 2001;11(2):160–4.
42. Yoshino N, Akimoto H, Yamada I, et al. Trigeminal neuralgia: evaluation of neuralgic manifestation and site of neurovascular compression with 3D CISS MR imaging and MR angiography1. Radiology 2003;228(2):539–45.
43. Chavhan GB, Babyn PS, Jankharia BG, et al. Steady-state MR imaging sequences: physics, classification, and clinical applications. Radiographics 2008;28(4):1147–60.
44. Shigematsu Y, Korogi Y, Hirai T, et al. Contrast-enhanced CISS MRI of vestibular schwannomas: phantom and clinical studies. J Comput Assist Tomogr 1999;23(2):224–31.
45. Taoka T, Hirabayashi H, Nakagawa H, et al. Displacement of the facial nerve course by

vestibular schwannoma: preoperative visualization using diffusion tensor tractography. J Magn Reson Imaging 2006;24(5):1005–10.
46. Chen DQ, Quan J, Guha A, et al. Three-dimensional in vivo modeling of vestibular schwannomas and surrounding cranial nerves with diffusion imaging tractography. Neurosurgery 2011;68(4):1077–83.
47. Lutz J, Linn J, Mehrkens JH, et al. Trigeminal neuralgia due to neurovascular compression: high-spatial-resolution diffusion-tensor imaging reveals microstructural neural changes. Radiology 2011; 258(2):524–30.
48. Fraher JP. The transitional zone and CNS regeneration. J Anat 1999;194(2):161–82.
49. Xenellis JE, Linthicum FH Jr. On the myth of the glial/schwann junction (Obersteiner-Redlich zone): origin of vestibular nerve schwannomas. Otol Neurotol 2003;24(1):1.
50. Jannetta PJ. Arterial compression of the trigeminal nerve at the pons in patients with trigeminal neuralgia. J Neurosurg 1967;26(Suppl 1):159–62.
51. Guclu B, Sindou M, Meyronet D, et al. Cranial nerve vascular compression syndromes of the trigeminal, facial and vago-glossopharyngeal nerves: comparative anatomical study of the central myelin portion and transitional zone; correlations with incidences of corresponding hyperactive dysfunctional syndromes. Acta Neurochir 2011;153(12):2365–75.
52. Kakizawa Y, Seguchi T, Kodama K, et al. Anatomical study of the trigeminal and facial cranial nerves with the aid of 3.0-tesla magnetic resonance imaging. J Neurosurg 2008;108(3):483–90.
53. Benes L, Shiratori K, Gurschi M, et al. Is preoperative high-resolution magnetic resonance imaging accurate in predicting neurovascular compression in patients with trigeminal neuralgia? Neurosurg Rev 2005;28(2):131–6.
54. Joo W, Yoshioka F, Funaki T, et al. Microsurgical anatomy of the abducens nerve. Clin Anat 2012; 25(8):1030–42.
55. McCabe JS, Low FN. The subarachnoid angle: an area of transition in peripheral nerve. Anat Rec 1969;164(1):15–33.
56. Janjua RM, Al-Mefty O, Densler DW, et al. Dural relationships of Meckel cave and lateral wall of the cavernous sinus. Neurosurg Focus 2008;25(6):1–12.
57. Kaufman B, Bellon EM. The trigeminal nerve cistern. Radiology 1973;108(3):597–602.
58. Ono K, Arai H, Endo T, et al. Detailed MR imaging anatomy of the abducent nerve: evagination of CSF into Dorello canal. AJNR Am J Neuroradiol 2004; 25(4):623–6.
59. Everton K, Rassner U, Osborn A, et al. The oculomotor cistern: anatomy and high-resolution imaging. AJNR Am J Neuroradiol 2008;29(7):1344–8.
60. Yousry I, Camelio S, Wiesmann M, et al. Detailed magnetic resonance imaging anatomy of the cisternal segment of the abducent nerve: Dorello's canal and neurovascular relationships and landmarks. J Neurosurg 1999;91(2):276–83.
61. Yousry I, Moriggl B, Schmid UD, et al. Trigeminal ganglion and its divisions: detailed anatomic MR imaging with contrast-enhanced 3D constructive interference in the steady state sequences. AJNR Am J Neuroradiol 2005;26(5):1128–35.
62. Yasuda A, Campero A, Martins C, et al. The medial wall of the cavernous sinus: microsurgical anatomy. Neurosurgery 2004;55(1):179–90.
63. Parkinson D. Extradural neural axis compartment. J Neurosurg 2000;92(4):585–8.
64. Umansky F, Valarezo A, Elidan J. The microsurgical anatomy of the abducens nerve in its intracranial course. Laryngoscope 1992;102(11): 1285–92.
65. Yagi A, Sato N, Taketomi A, et al. Normal cranial nerves in the cavernous sinuses: contrast-enhanced three-dimensional constructive interference in the steady state MR imaging. AJNR Am J Neuroradiol 2005;26(4):946–50.
66. Linn J, Peters F, Lummel N, et al. Detailed imaging of the normal anatomy and pathologic conditions of the cavernous region at 3 Tesla using a contrast-enhanced MR angiography. Neuroradiology 2011; 53(12):947–54.
67. Davagnanam I, Chavda S. Identification of the normal jugular foramen and lower cranial nerve anatomy: contrast-enhanced 3D fast imaging employing steady-state acquisition MR imaging. AJNR Am J Neuroradiol 2008;29(3):574–6.
68. Linn J, Peters F, Moriggl B, et al. The jugular foramen: imaging strategy and detailed anatomy at 3T. AJNR Am J Neuroradiol 2009;30(1):34–41.
69. Zhang Z, Meng Q, Chen Y, et al. 3-T imaging of the cranial nerves using three-dimensional reversed FISP with diffusion-weighted MR sequence. J Magn Reson Imaging 2008;27(3):454–8.
70. Akter M, Hirai T, Minoda R, et al. Diffusion tensor tractography in the head-and-neck region using a clinical 3-T MR scanner. Acad Radiol 2009;16(7): 858–65.